Astronomy & Astrophysics manuscript no. final
March 2, 2022
©ESO 2022

arXiv:1803.00614v1 [astro-ph.SR] 1 Mar 2018

Multi-epoch monitoring of the AA Tau like star V 354 Mon

Indications for a low gas-to-dust ratio in the inner disk warp

P. C. Schneider[1,2], C. F Manara[2,3], S. Facchini[4], H. M. Günther[5], G. J. Herczeg[6], D. Fedele[7], and P. S. Teixeira[8,9,10]

[1] Hamburger Sternwarte, Gojenbergsweg 112, 21029 Hamburg, Germany, e-mail: astro@pcschneider.eu
[2] Scientific Support Office, Directorate of Science, European Space Research and Technology Center (ESA/ESTEC), Keplerlaan 1, 2201 AZ Noordwijk, The Netherlands
[3] European Southern Observatory, Karl-Schwarzschild-Str. 2, D-85748 Garching bei München, Germany
[4] Max-Planck-Institut für extraterrestrische Physik, Gießenbachstrasse 1, Garching bei München
[5] Massachusetts Institute of Technology, Kavli Institute for Astrophysics and Space Research, 77 Massachusetts Avenue, Cambridge, MA 02139
[6] Kavli Institute for Astronomy and Astrophysics, Peking University, Yiheyuan 5, Haidian Qu, 100871 Beijing, People's Republic of China
[7] INAF - Osservatorio Astrofisico di Arcetri, Largo E. Fermi 5, 50125, Firenze - Italy
[8] Institut für Astrophysik, Universität Wien, Türkenschanzstrasse 17, 1180 Vienna, Austria
[9] Institut de Ciències del Cosmos (ICCUB), Universitat de Barcelona (IEEC-UB), Martí Franquès 1, E08028 Barcelona, Spain
[10] Scottish Universities Physics Alliance (SUPA), School of Physics and Astronomy, University of St. Andrews, North Haugh, St. Andrews, Fife KY16 9SS, UK

received; accepted

ABSTRACT

Disk warps around classical T Tauri stars (CTTSs) can periodically obscure the central star for some viewing geometries. For these so-called AA Tau-like variables, the obscuring material is located in the inner disk and absorption spectroscopy allows one to characterize its dust and gas content. Since the observed emission from CTTSs consists of several components (photospheric, accretion, jet, and disk emission), which can all vary with time, it is generally challenging to disentangling disk features from emission variability. Multi-epoch, flux-calibrated, broadband spectra provide us with the necessary information to cleanly separate absorption from emission variability. We applied this method to three epochs of VLT/X-Shooter spectra of the CTTS V 354 Mon (CSI Mon-660) located in NGC 2264 and find that: (a) the accretion emission remains virtually unchanged between the three epochs; (b) the broadband flux evolution is best described by disk material obscuring part of the star, and (c) the Na and K gas absorption lines show only a minor increase in equivalent width during phases of high dust extinction. The limits on the absorbing gas column densities indicate a low gas-to-dust ratio in the inner disk, less than a tenth of the ISM value. We speculate that the evolutionary state of V 354 Mon, rather old with a low accretion rate, is responsible for the dust excess through an evolution toward a dust dominated disk or through the fragmentation of larger bodies that drifted inward from larger radii in a still gas dominated disk.

Key words. Stars: individual: V354 Mon, Stars: low-mass, stars: pre-main sequence, stars: variables: T Tauri, Herbig Ae/Be, X-rays: stars, Infrared: stars, Protoplanetary disks

1. Introduction

Young stars are surrounded by copious amounts of circumstellar gas and dust. A fraction of this material survives the main accretion phase and can still surround the young star after a few million years in the form of a circumstellar disk, which might evolve into a debris disk dominated by reprocessed dust grains. The structure of protoplanetary disks is currently subject to intense observational and theoretical investigations, often focusing on intrinsic disk emission (Nomura et al. 2016; Ansdell et al. 2016; Cox et al. 2017; Loomis et al. 2017; Long et al. 2017).

An alternative to these disk emission studies is absorption spectroscopy. So-called AA Tau-like variables show periodic dips in their light curves (e.g., Bouvier et al. 1999, 2007; McGinnis et al. 2015). These dips are thought to be caused by warps in the inner disk that rotate between the star and the observer so that the line of sight periodically passes through the warp. Hence, differential absorption spectroscopy provides us with the properties of the obscuring material, i.e., the inner disk material that is currently unaccessible by (interferometric) imaging techniques. The periods of the dips are typically five to ten days, which translates to radii of about 0.1 au assuming Keplerian rotation. Hence, the warp material is close to or even cospatial with the inner disk edge. Figure 1 sketches the envisaged geometry, which naturally results from the interaction between the stellar magnetic field and the inner disk edge (Foucart & Lai 2011).

A related, perhaps overlapping, class of objects are the so-called dippers (Stauffer et al. 2015). Their light curves bear many similarities to those of AA Tau-like objects, but the dips are less pronounced and shallower than for those of "classical" AA Tau-like objects. For both types of light curves, material at the inner disk edge is responsible for the dimmings. However, it is somewhat unclear if these two types of light curves really describe two different phenomena (e.g., a persistent disk "wall' vs. intermittent material in the disk atmosphere) or rather the same mechanism but of variable strength (e.g., variable filling of a warped inner disk atmosphere). Recent studies show that the in-

ner and outer disks are not necessarily aligned (Ansdell et al. 2016; Scaringi et al. 2016) and absorption by inner disk material is also observed in systems with rather inclined outer disks, including the prototypical AA Tau system, where ALMA observations of dust in the outer disk reveal a disk inclination of about 59°, meaning they are decidedly not close to edge-on (Loomis et al. 2017).

Specifically for the AA Tau system, no strong color changes during the eclipses have been found. In other words, the extinction is rather gray, which suggests that the extinction is caused by large grains in the line of sight (Bouvier et al. 2003). However, accretion variability can also change the observed stellar spectrum. Due to disk-locking (e.g., Matt et al. 2010), the stellar period and the rotation period of the inner disk warp are likely (almost) synchronized so that it is challenging to disentangle accretion and extinction properties using photometry only.

Further, the disk warps are not stable and changes in the inner disk geometry are the preferred explanation for major dimming events of CTTSs. Examples of these dimming events are AA Tau (Bouvier et al. 2013; Schneider et al. 2015a), RW Aur (Petrov et al. 2015; Schneider et al. 2015b; Bozhinova et al. 2016; Facchini et al. 2016) as well a few other objects (Hamilton et al. 2001; Rodriguez et al. 2015, 2017). Combining the findings from these studies, which use information from X-ray to NIR wavelengths, shows that the dimming events are likely caused by perturbations in the inner disk with a scale height of about one stellar radius and that the material has a gas-to-dust ratio close to the ISM value.

Here, we present flux-calibrated X-Shooter spectra of the CTTS V354 Mon to measure simultaneously (a) accretion signatures using line fluxes, (b) dust extinction through changes in the broadband spectral energy distribution (SED), and (c) changes in the absorbing gas column density from inspection of strong absorption lines. Our paper is structured as follows. The target, V 354 Mon, is described in Sect. 2. The X-Shooter observations are described in Sect. 3 and we present our results in Sect. 4. In Sect. 5 we provide a brief discussion of our results and we close with the conclusions in Sect. 6.

2. V 354 Mon

The CTTS V 354 Mon (or CSI Mon-660) is located in NGC 2264 (d=760 pc, Dahm 2008) and has been extensively studied in the framework of the CSI NGC 2264 project (e.g., Alencar et al. 2010). Specifically, McGinnis et al. (2015) classify V 354 Mon as a stable AA Tau-like variable with a period of 5.25 days where "stable" indicates that regular eclipses with a depth of about 1 mag are present during both CoRoT observing epochs (2008 and 2011) of approximately one month length each.

Fonseca et al. (2014) present a detailed study of V 354 Mon using photometry and Hα profiles covering about two rotation periods. They correlate the flux evolution with absorption features seen against the Hα line and find that redshifted absorption is most pronounced during the epoch of the lowest flux. Fonseca et al. (2014) suggest that an accretion funnel causes the redshifted Hα absorption with the hotspot located under the funnel facing the observer during the phase of the flux minimum. Furthermore, they find that a hotspot cannot contribute significantly to the observed spectrum. Instead, they model the (approximately sinusoidal) evolution of the photometric magnitudes as variable circumstellar material, i.e. a disk warp, which extends about $h/r = 0.3$ above the disk midplane (h and r being the height above the disk midplane and the inner disk radius, respectively). Here, we want to use exactly this property, the modulation of the observed stellar flux due to circumstellar material, to obtain further insight into the composition of the disk material.

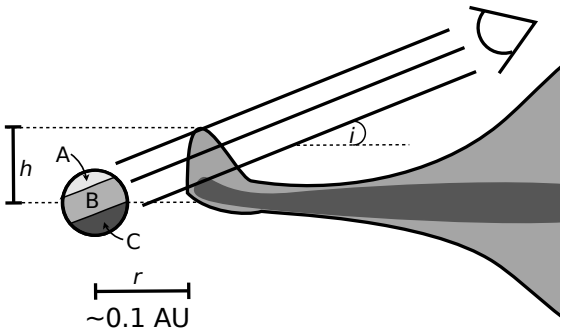


Fig. 1. Sketch of the inner disk structure around CTTSs indicating our three component model. The unocculted part of the stellar disk is denoted with *A*. The upper disk layer causes reddening of part the stellar disk (part *B* of the stellar disk). Stellar emission from the region denoted with C is subject to opaque (gray) extinction by the lower disk layers. We also show the inner disk radius r, the viewing inclination i, and the height h of the inner disk warp with respect to the disk midplane.

3. Observations and data analysis

The star V 354 Mon was selected based on the known variability in previous CoRoT observations. Observations were performed over three consecutive nights in 2010 with X-Shooter at airmasses between 1.21 and 1.27. Table 1 provides an overview of the observations and Fig. 3 shows the flux calibrated spectra. The spectral region covered by X-Shooter ($\lambda\lambda$ ~300-2500 nm) is observed simultaneously and the spectra are divided into three arms, UVB ($\lambda\lambda$ ~ 300-550 nm), VIS ($\lambda\lambda$ ~ 550-1010 nm), and NIR ($\lambda\lambda$ ~ 1010-2500 nm). Observations were carried out using the narrower slits in the VIS and NIR arms (0.″4 width) and the 1″ wide slit in the UVB arm. Before the exposures with the narrow slits, a short exposure with a slit width of 5″ width was performed in order to account for slit losses and to spectrophotometrically calibrate the spectra. The spectra were acquired by nodding the telescope along a direction perpendicular to the slit and the nebular and sky emission was subtracted when combining the four nodding frames. Data reduction follows the same procedure as in Manara et al. (2016). Briefly, the spectra were reduced with the ESO X-Shooter pipeline version v.1.3.2 (Modigliani et al. 2010). The 1D spectra were manually extracted from the rectified 2D spectra produced by the pipeline. Flux calibration was performed using observations of the spectrophotometric standard stars GD-71 (observed at the beginning of each night) and Hiltner-600 (observed every one to two hours each night). Finally, the narrow-slit spectra were rescaled upward to match the large-slit spectra (see Rugel et al. 2018, for a detailed discussion of the accuracy and stability of the flux calibration method). The VIS arm was corrected for telluric absorption lines using a telluric standard star observed close in time and airmass to the target. We derived the stellar, heliocentric rest velocity as $18.6 \pm 1.0\,\mathrm{km\,s^{-1}}$ from fitting the Li λ671 line, which is compatible with the velocity of the NGC 2264 cloud (Fűrész et al. 2006).

The X-Shooter spectra include atomic gas absorption lines, which we fit with Voigt-profiles using PyAstronomy[1]. Specifically, we allowed the central wavelengths, line amplitudes and line widths to vary during the fit. We estimated the local error by the standard deviation in presumably line-free wavelength regions and provide 1 σ errors. Further, we required the two members of the doublets under consideration to have the same width. The equivalent width (EW) is derived from this fit to provide reasonable errors (we used Markov chain Monte Carlo methods and 5×10^4 iterations). These values agree well with the EW derived from direct integration.

Our analysis is differential and most values are measured with respect to the brightest spectrum (2010-01-20). To simplify the discussion, we have assumed in the following that the brightest spectrum corresponds to the uneclipsed star. If the brightest spectrum is already subject to partial circumstellar extinction, our conclusions change only in so far that the values should be corrected for the difference between the brightest spectrum and the uneclipsed star.

4. Results

We first derived the stellar parameters and accretion properties from the brightest spectrum (2010-01-20), which has a V magnitude that is within 0.1 mag of the value quoted in Fonseca et al. (2014), meaning that it is virtually equal to the uneclipsed spectrum. The two other spectra are dimmer by 0.5 mag (2010-01-19) and 1.0 mag (2010-01-18) in the V band. We note that extrapolating the CoRoT data[2] places the 2010-01-18 spectrum close to flux maximum, which also explains the choice of integration times. This is contrary to our data, but already a minor change in period of only 0.02 days (fully compatible with the combined 2008+2011 CoRoT dataset) shifts the disk warp phases associated with the X-Shooter observing dates by half a period. Hence, the X-Shooter data are fully compatible with an unchanged disk warp period.

4.1. Stellar parameters and accretion

For reference, we started by fitting the brightest spectrum with a combination of synthetic spectra, accretion emission, and absorption using the methodology of Manara et al. (2013); Alcalá et al. (2014). We find a spectral type of K2 ($T_{\rm eff}$ = 4900 K, close to K4 derived by Fonseca et al. 2014), $M_\star \sim 1.4 - 1.5\,M_\odot$ and a quite large age of $\sim$ 7 Myr for the Siess et al. (2000) evolutionary tracks, which is somewhat older than the age of 3 Myrs derived by Lamm et al. (2004) and Flaccomio et al. (2006). The corresponding stellar radius is about $1.8\,R_\odot$ while Fonseca et al. (2014) estimate $R_\star = 2.4\,R_\odot$. The difference is mainly caused by a slightly lower T_{eff} assumed by Fonseca et al. (2014). We used these values to provide phtospheric EWs for reference and to transfer orbital periods to radii, but our key diagnostics are entirely differential between the three individual spectra so that the exact values are of minor importance. Still, we note that the values for V 354 Mon recently published by Venuti et al. (2018) agree quite well with our values (T_{eff} = 4836 K, A_V=0.76, $L_{bol} = 1.964\,L_\odot$, $M_\star = 1.59\,M_\odot$, EW(Hα) = 1.2 Å).

Assuming that the brightest spectrum is only subject to interstellar reddening we find A_V = 0.7 mag for R_V = 3.1 and the Cardelli et al. (1989) reddening law. The best fit requires some excess in the blue part of the spectrum, which corresponds to $L_{excess}/L_\star \approx 0.22\,L_\odot/1.67\,L_\odot \approx 0.13$. Interpreting this excess as accretion would imply an accretion rate $\dot{M}_{acc}$ of about $2 \times 10^{-8}\,M_\odot$/yr, which is a typical value for CTTSs with the stellar mass of V 354 Mon. However, the other epochs do not require excess blue emission, and emission line fluxes that usually go along with such accretion rates are not seen in any epoch. In fact, most of the accretion tracers do not have significant negative equivalent widths, let alone fluxes expected for an accre-

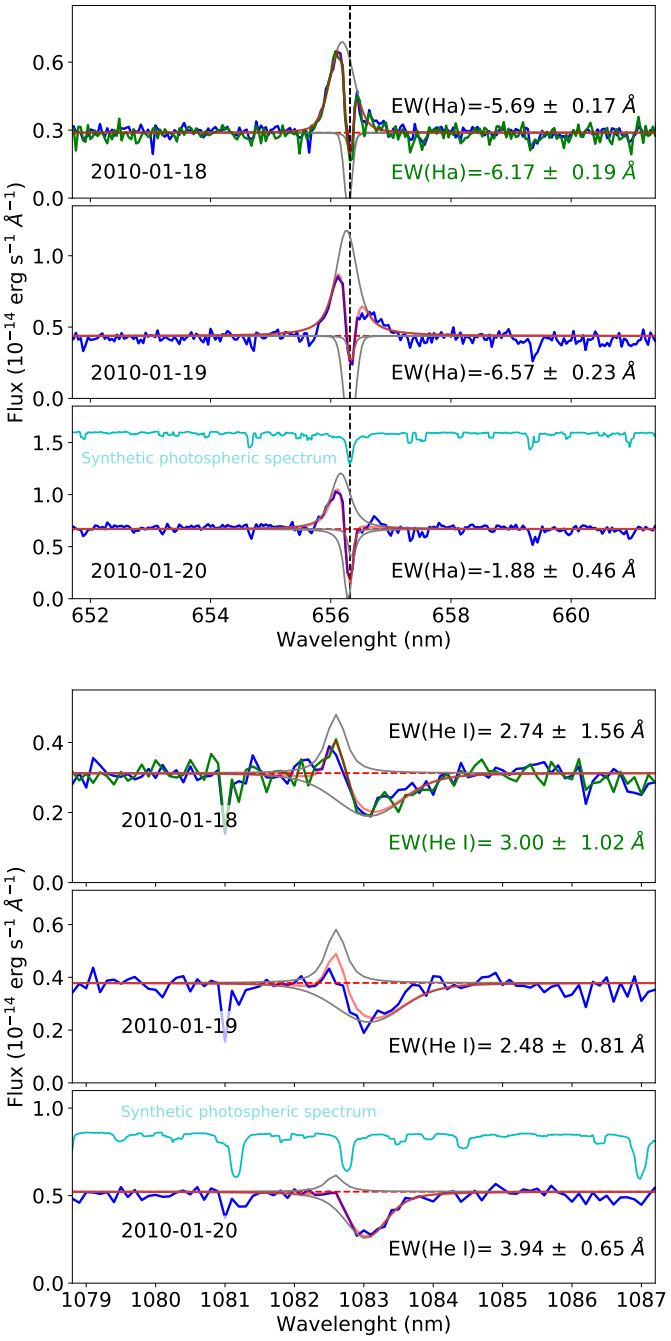


Fig. 2. Top: Hα spectra fitted with a two component model (one emission, one absorption Voigt-profile) including a stellar absorption component. **Bottom**: He I spectra fitted with a two component model (one emission, one absorption Voigt-profile). Individual fit-components are shown in gray. The synthetic spectrum is offset for clarity.

[1] https://github.com/pcschneider/PyAstronomy

[2] "Transit" center: MJD = 54534.22 or JD=2454534.72, i.e., time of max. disk absorption; orbital period: 5.25 days (from McGinnis et al. 2015).

Table 1. Observing details

Date Jan. 2010	JD (2455000+)	ObsID	t_{exp} (s)	Airmass
18th 02:21:51	214.59	200198250	80	1.27
18th 02:32:23	214.60	200198252	50	1.26
19th 03:12:39	215.63	200198321	50	1.21
20th 02:40:46	216.62	200198391	120	1.23

tion rate of $\dot{M}_{acc} \sim 10^{-8}\,M_\odot\,\mathrm{yr}^{-1}$. Only H$\alpha$ is significantly in emission during all epochs (Fig. 2, $EW = -7 \cdots -2$ Å), but its EW falls well short of the expection based on an accretion rate of $10^{-8}\,M_\odot\,\mathrm{yr}^{-1}$ (Hα EW expected > 100 Å, see Alcalá et al. 2014). Furthermore, the Hα EW is lowest during the brightest epoch (consistent with the findings of Fonseca et al. 2014).

The Hα profiles show a strong absorption feature close to the stellar rest velocity (Fig. 2). Modeling the Hα profile with two Voigt profiles, this absorption component is redshifted with respect to the emission component by about $24\,\mathrm{km\,s}^{-1}$ although the exact velocity difference is somewhat uncertain due to the cross-talk between absorption and emission. There are no significant differences in the ratios between the amplitudes of the absorption and emission component. The flux in the emission component of the Hα line ($\approx 10^{30}\,\mathrm{erg\,s}^{-1}$) points to accretion rates $\lesssim 10^{-10}\,M_\odot\,\mathrm{yr}^{-1}$ (e.g., Dahm 2008; Alcalá et al. 2014), compatible with the other emission lines. Also, the depth of photospheric lines does not change between the epochs (see Fig. B.1), which would be expected if strong accretion variability were present. Therefore, we do not consider the blue excess in just one epoch as indicative of strong accretion, but rather as an artifact of the fitting procedure given the potentially complex circumstellar structure.

We also inspected the He I lines (at 588 nm and 1 μm) in an attempt to correlate redshifted absorption and disk warp phase similar to the investigation by Fischer et al. (2008) for AA Tau. For V 354 Mon, the redshifted absorption component of the He I 1 μm line shows an approximately 10 % increase in the EW between the dimmest and the brightest spectrum (see Table 3) while the data for He I λ588 nm is insufficient to draw solid conclusions on its EW evolution. In any case, the observed changes are considerably smaller than those observed for AA Tau by Fischer et al. (2008), where the EW increased from 0.4 to 4.4 Å within a similar range of disk warp phases. Taken at face value, the V 354 Mon trend also goes into the opposite direction, i.e., the largest EW pertains to the brightest spectrum contrary to the findings by Fischer et al. (2008) for AA Tau. We caution, however, that the minor changes observed for the He I EW in V 354 Mon could be additionally affected by an interplay with the weak emission component that is spectrally not well resolved by X-Shooter. Therefore, we refrain from a detailed investigation noting only that the lack of a strong change in the He I absorption and the difference to AA Tau is entirely compatible with the derived low accretion rate and the associated lack of strong absorption by the accretion funnel in He I.

In summary, signatures of strong accretion are not significantly detected; emission from the accretion shock is negligible in shaping the observed spectra compared to absorption effects, which agrees with the interpretation by Fonseca et al. (2014). Thus, we interpret the flux evolution observed in the X-Shooter spectra as an effect of variable circumstellar absorption.

Table 2. Results of the spectral fitting. A_V is derived as the change in V-band magnitude caused by the reddening and not part of the fitting procedure.

Parameter	Value 2010-01-19	2010-01-18
Extinction only (blue lines in the bottom two panels of Fig. 3)		
$E(B-V)$	0.08	0.19
R_V	8.0	6.0
A_V (derived)	0.62	1.16
AA Tau model w/ $R_V = 3.1$ (red lines in the bottom two panels of Fig. 3)		
$E(B-V)$	0.69 ± 0.11	0.53 ± 0.07
A_V	0.45	0.96
reddened (S_B)	0.38 ± 0.02	0.64 ± 0.07
unobscured (S_A)	0.54 ± 0.02	0.23 ± 0.04

4.2. Dust extinction

Here we investigate the flux evolution and model it as an extinction effect since there are no indications for veiling changes due to accretion variability. We find that changing only the extinction between the epochs cannot explain the differences between the spectra even when allowing $E(B-V)$ to vary freely and R_V to vary between two and eight. The blue part of the spectrum would be underpredicted while the flux at longer wavelengths would be overpredicted, meaning that the predicted SED for the dimmer spectra is too red compared the observed flux although we allow for exceptionally large values of R_V (see Fig. 3).

Extending the extinction-only model with a gray absorption component does not resolve the discrepancies. However, this model allows us to check the possibility of a significant scattering contribution as follows. First, we restricted the fit to wavelengths longward of 8000 Å where scattering should be less important than at shorter wavelengths. Second, we performed a fit allowing $E(B-V)$, R_V and the gray extinction part to vary. While this model provides a reasonable fit to the red spectral evolution, it underpredicts the flux at blue wavelengths. This is exactly the part of the spectrum in which we would expect scattering to contribute. However, about 15 % of the flux in the bright state would be required to provide the missing flux. Such a high scattering efficiency is very unlikely given that a "standard" protoplanetary disk intercepts only about 10 % of the stellar light, so we ignore scattering in the following. We note, however, that scattering can modify the derived values (slightly). Most of the missing blue flux must come from a different source: the fraction of the star that is not eclipsed by the disk warp as detailed in the following.

Next, we considered a mathematical description for the flux evolution that represents the physical model sketched in Fig. 1, which is based on the AA Tau scenario (e.g., Bouvier et al. 2003; Schneider et al. 2015a). We assumed that the absorption is caused by a warp in the inner disk that grazes the stellar disk. The warp's linear dimensions are on the order of the stellar radius to obscure a sufficient fraction of the stellar emission. Specifically, we modeled the flux evolution as a combination of (A) the unocculted star, (B) the upper layers of the disk characterized by reddening according to the Cardelli et al. (1989) extinction law, and (C) gray absorption caused by the lower disk layers, i.e.,

$$\text{Observed Spec.} = S_A F_{\text{direct}} + S_B F_{\text{reddened}} + S_C F_0\,, \quad (1)$$

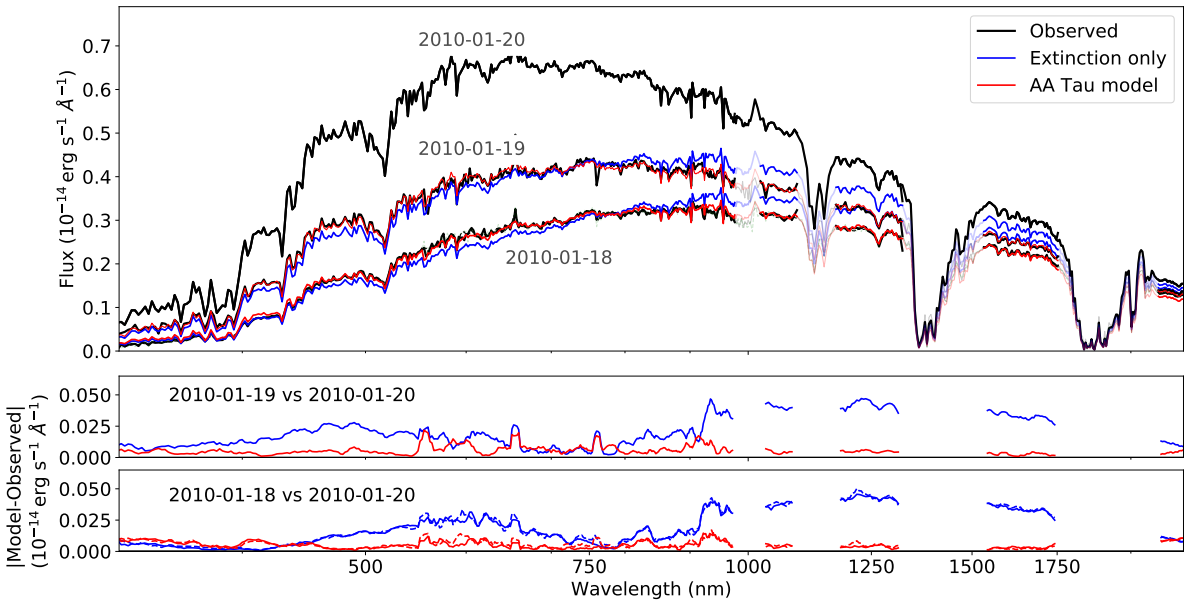


Fig. 3. Top: Observed spectral energy distributions. **Bottom** two panels: Absolute difference between model and observed spectra. Models for the dimmer spectra (18th and 19th Jan.) assume that the difference between the brightest spectrum (20th Jan.) and the dimmer spectra is caused (1) only by additional extinction allowing $E(B-V)$ and R_V to vary (blue), and (2) our AA Tau model in red (see text for a detailed description). To differentiate between the two 18th Jan. spectra, the shorter one is displayed as a dashed line. Spectral ranges strongly affected by telluric absorption are removed from the fit and shown in lighter colors. The parameters corresponding to the blue and red curves in the bottom two panels are given in Table 2.

where S_A, S_B, and S_C are the fractional visible surface areas of the regions A, B, and C from Fig. 1, and $F_{\rm direct}$, $F_{\rm reddened}$, and F_0 are the direct, reddened, extinguished ($F_0 = 0$) spectra, respectively. We require that $S_A + S_B + S_C = 1$. This model is intended as a simplified representation of the warp, which likely has a continuous structure. We allowed R_V to vary, but find that it's value is consistent with the canonical value of 3.1; and therefore decided to fix it to $R_V = 3.1$ in the following. The resulting fit parameters are listed in Table 2. The fit shows that the

- fraction of the stellar surface covered by the extra absorber increases (38 and 64 % covering fractions),
- directly viewed stellar surface decreases (54 and 23 %),
- reddening, $E(B-V)$, decreases slightly,
- and that the gray extinction increases (8 and 13 % covering fractions)

with decreasing flux. Thus, the flux evolution can be well explained by a warp rotating into view and partially occulting the stellar photosphere.

Assuming that the 20th Jan. spectrum represents the uneclipsed star, we can transfer these values to physical lengths using the geomtrical relations between inclination i, disk warp height h, inner disk radius r, and stellar radius $R_\star$ as shown in Fig. 1. Specifically, we used an inclination of about 80° and $6\,R_\star = 10^{12}$ cm for the radius of the warp (estimated from the dip period and using $R_\star \approx 2.37\,R_\odot$, see Fonseca et al. 2014). The opaque part of the warp extends 0.37 and $0.26\,R_\star$ above the midplane (for the Jan. 18. and 19. spectra, resp.) while the part of the warp causing reddening extends 1.07 and $0.68\,R_\star$ above the disk midplane (for the Jan. 18. and 19. spectra, resp.). The CoRoT light curves indicate that the warp blocks part of the star during about half of the rotation period, which points to a ratio of roughly 3:1 between the azimuthal and vertical dimensions of the warp given the above size estimate. We note that, with the viewing geometry derived by Fonseca et al. (2014), the star is unobscured only during phases when the disk does not significantly extend above the disk midplane.

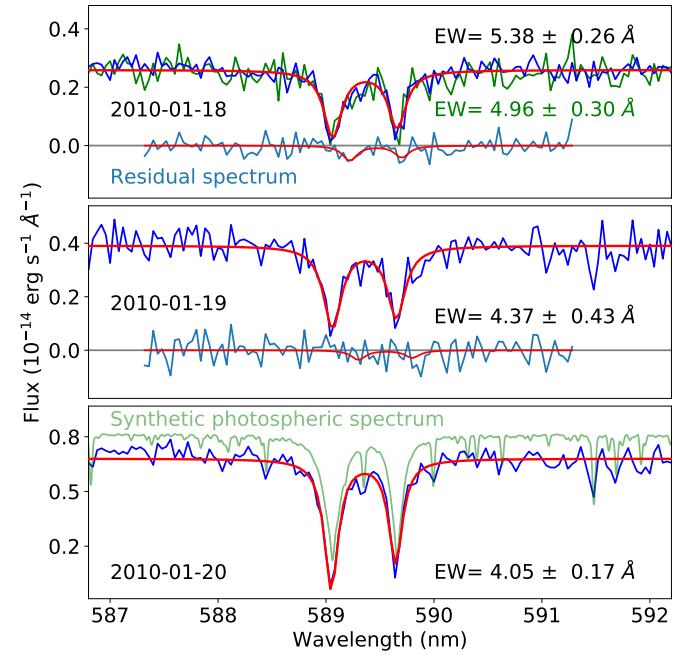
Table 3. Summary of measured line properties (EWs for 2010-01-18 are error-weighted averages).

Line		EW (Å)		
	(nm)	2010-01-18	2010-01-19	2010-01-20
Hα	656	-5.90 ± 0.18	-6.57 ± 0.23	-1.88 ± 0.46
Na	589+589.6	5.24 ± 0.24	4.37 ± 0.43	4.05 ± 0.17
K	766+770	1.00 ± 0.08	0.89 ± 0.08	0.85 ± 0.03
Li	671	0.47 ± 0.02	0.44 ± 0.04	0.50 ± 0.02
He I[a]	1083	5.01 ± 0.80	4.11 ± 0.67	4.39 ± 0.56

Notes. [(a)] Absorption component only. The integrated He I EW is provided in Fig. 2.

4.3. Gas absorption

The X-Shooter spectra also contain atomic gas absorption lines that include nonstellar contributions, which we later correlate with the dust extinction. The spectral resolution of X-Shooter renders it challenging to differentiate interstellar (expected to be narrow) from circumstellar absorption (expected to be broad) directly in the spectra. Hence, we concentrated on the evolution of the observed EW, because any "truly" interstellar (e.g., Pascucci et al. 2015) or stellar absorption is expected to stay constant. In this situation, observable changes in the absorption require that inter- and circumstellar column densities have roughly similar values. Circumstellar column density changes that are small compared to the interstellar absorption would remain unnoticed. Conversely, observing EW changes directly implies that the circumstellar column densities are sufficiently large.



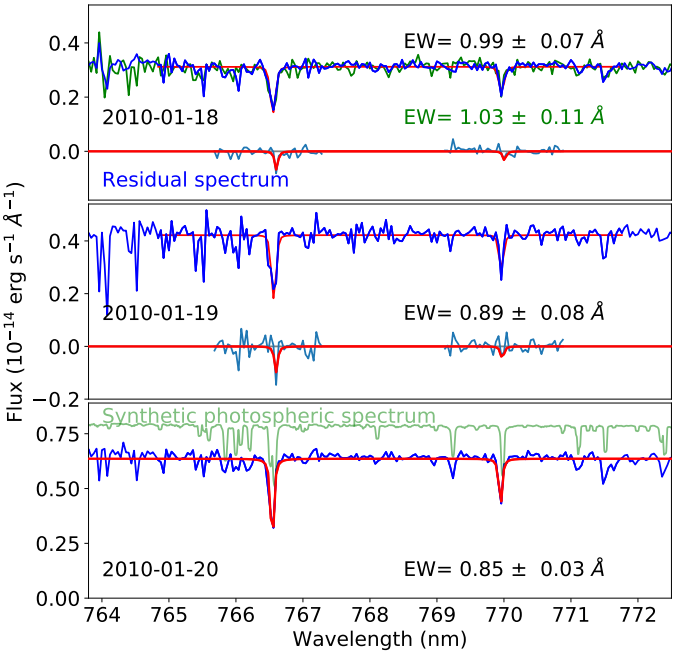


Fig. 4. Top: Na absorption lines. **Bottom**: K absorption lines. The photospheric spectrum is based on the PHOENIX model described in the text. The residual spectrum is the spectrum minus the brightest spectrum (2010-01-20, the brightest spectrum was normalized to the same continuum level prior to subtraction, the two 2010-01-18 spectra were averaged prior to subtraction). The fit is shown in red (only for the longer spectrum from 20th Jan. for clarity).

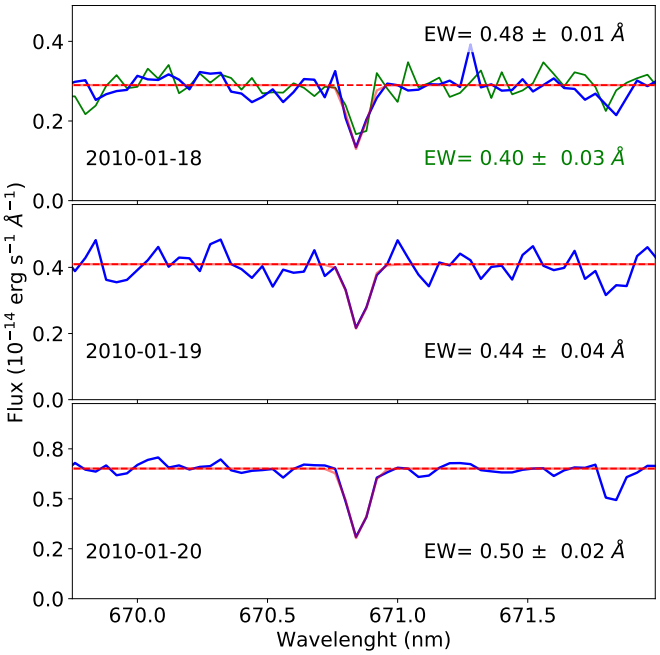


Fig. 5. Li absorption line. The fit is shown in red (only for the longer spectrum from 20th Jan. for clarity).

4.3.1. Measured line properties

The Na and K optical doublets are the strongest absorption lines in our spectra (Fig. 4). They are common interstellar absorption lines (e.g., Welty & Hobbs 2001), but can also have circumstellar contributions. In fact, accretion emission can also contribute to these lines, but the lack of strong accretion signatures[3] implies that this would affect the EW by $\lesssim 10$ mÅ. Similarly, absorption by the accretion funnels has been suggested to cause broad absorption features in CTTS, mainly in the strongly accreting ones. Hence, we regard a funnel contribution to the Na and K absorption insignificant for V 345 Mon due to its very low accretion rate.

In all three epochs, we clearly detect absorption in the Na and K optical doublets while the Na UV lines are not significantly detected with a combined EW upper limits of 0.7 Å. The depth of the Na and K doublets is mainly photospheric, the PHOENIX model (T_{eff} = 4900 K, log g = 4.50, solar metallicity, see Husser et al. 2013) gives stellar EWs of 3.6 Å (Na) and 0.6 Å (K). Neverthless, material between us and the photosphere causes extra and variable absorption since the measured EW is higher than the photospheric value for both doublets during all epochs. With the limited spectral resolution of X-Shooter, we cannot localize the gas that causes this extra absorption, for example, through its velocity structure. However, some of this extra absorption is likely interestellar and thus constant between the observing nights (Pascucci et al. 2015). As we regard the accretion process in V 354 Mon to have an insignificant effect on the Na and K lines, the variable gas absorption is likely associated with material in the (inner) disk region.

We provide the EWs in Table 3 and note that the fitted line widths as well as the line ratios (measured mean 1.2 ± 0.1 for Na and 2.0 ± 0.2 for K) are similar in all epochs. We are particularly interested in the EW change, because it is related to variable amounts of circumstellar material. We denote this value as ΔEW. Specifically, we find an increase in Na EW of $\Delta EW = 1.2 \pm 0.3$ Å (for 2010-01-18 → 2010-01-20) and $\Delta EW = 0.3 \pm 0.4$ AA (2010-01-19 → 2010-01-20). The increases in K EWs are 0.15 ± 0.08 Å (for 2010-01-18 → 2010-01-20) and 0.04 ± 0.08 Å (for 2010-01-19 → 2010-01-20), respectively. The data are insufficient to detect a deviation of the blue-to-red line ratio between the epochs.

[3] The Hα flux indicates $\log L_{acc}/L_\odot < -2.5$ and $\log L(NaI)/L_\odot = -5.5$.

4.3.2. Column densities

The conversion from ΔEW to column density depends on the properties of the absorbing material like temperature and ionization fraction. Specifically for V 354 Mon, the conversion also depends on the covering fraction of the absorbing layer since the absorber does not cover the entire stellar surface. Correcting for the fact that the absorber covers only 65 % of the visible stellar surface (2010-01-18), we find that circumstellar material causes up to $\Delta EW = 1.8 \pm 0.5$ Å (Na) and 0.2 ± 0.1 Å (K).

We now consider the properties of the absorbing material assuming that the same gas causes the Na and K absorption. At a radius of 0.1 au, the gas temperature is expected to be about 1400 K (equivalent to 0.1 eV) so that both, Na and K, are neither significantly thermally ionized (the energies of the first ionization potentials are 4.3 eV and 5.1 eV for Na and K, resp.) nor is the upper level significantly thermally populated (excitation energies are 2.1 eV and 1.6 eV, for Na and K respectively).

Photoionization, however, can cause non-negligible ionization in parts of the innermost fraction of the disk rim. While a detailed photo-chemical simulation is beyond the scope of this paper, we ran several simple cloudy simulations (Ferland et al. 2013) to estimate the impact of photoionization. Specifically, we reconstructed the stellar emission from available observations across the electromagnetic spectrum as detailed in Appendix B. We used a cylindrical geometry with height and radial extent of 0.1 au, a fixed temperature of 1400 K, and densities such that they reproduce the observed extinction ($\log n \sim 8$, grain abundance $\gtrsim 10\times$ISM). These experiments suggest that photoionization might cause a volume averaged ionization somewhere between 10 and about 90 percent. In the following, we present values assuming no photoionization noting that these are lower limits and the total Na and K column densities might be up to a factor of ten higher.

We now continue estimating the Na and K column densities. Optical depth effects are less pronounced for K. The line ratio of about two for the K doublet[4] suggests $N_K = 1.1 \times 10^{12}\,\mathrm{cm}^{-2}$ based on $\Delta\,\mathrm{EW} = 0.2$ Å. For Na, we assumed that the measured line ratio of 1.3 holds also for the extra circumstellar absorber and use Table 2 in Strömgren (1948) to find $N_{Na} \approx 3\times10^{13}\,\mathrm{cm}^{-2}$, surprisingly close to the value expected based on the K column density and their elemental abundance ratio. Both values correspond to $N_H \approx 1\ldots2\times10^{19}\,\mathrm{cm}^{-2}$ if Na and K in the disk warp are neutral.

To provide a rough estimate of the gas density in the disk warp located at ~ 0.1 au, we assumed that the length of the sightline through the warp is 0.1 au. Assuming a Keplerian disk, differential rotation would quickly shear apart any structure that extends over substantially different radii unless the structure is maintained or supported by other processes[5]. This gives a density of $n_H \sim 10^7\,\mathrm{cm}^{-3}$ in the warp. This value cannot be easily converted to a disk surface density since we do not probe the part of the disk causing the opaque obscuration, where the dust density is higher.

[4] Strictly speaking, this applies only for the combination of photospheric, inter-, and circumstellar absorption. However, we do not find indications for a change in the line ratio for the difference spectrum.

[5] This likely also holds if the warp is caused by the interaction of the disk with the stellar magnetic field as the magnetic field strength decreases with r^3, i.e., the field strength at 0.1 au is almost a magnitude higher than at 0.2 au.

4.4. Dust vs. gas

The ratio of gas to dust absorption is $\Delta N_H = 1\ldots2\times10^{19}\,A_V^{-1}$ (we transferred the modeled $E(B-V)$ to A_V using $R_V = 3.1$). This is a factor of 100 below the interstellar value for a gas-to-dust ratio of 100:1 and implies a strong overabundance of dust in the warp or a strong depletion of neutral, atomic Na and K. Considering a possible (photo-) ionization of the gas in the disk warp, the true (total) gas-to-dust ratio might be as low as about 10:1, which still implies a dust overabundance albeit less severe than in the situation assuming dominantly neutral Na and K.

5. Discussion

We find large differences between the spectra of V 354 Mon obtained in three consecutive nights. The broadband evolution of the SED is dominated by dust extinction. A combination of light from the unocculted star, from a reddened stellar spectrum, and gray extinction accurately describes the flux evolution for wavelengths between 300 and 2000 nm. Specifically, we find that with decreasing flux both the fraction of the star obscured by the gray absorber as well as the fraction of the star subject to reddening increase while the fraction of the star that remains unobscured decreases.

We also find an evolution in atomic absorption lines with the dimmest spectrum exhibiting the largest EW. The variability amounts to a quarter of the total EW, which we ascribe to circumstellar gas. The change in the neutral gas column densities is small compared to expectations based on interstellar conditions, and photo-ionization is not likely to make up for the missing gas. This raises the question as to whether our analysis strategy misses significant amounts of gas or overestimates the intervening dust and we consider (1) the doublet's line ratio, (2), elemental abundances, and (3) an underestimate of the ionization as possible causes for a low gas column density in the following.

First, we used the doublet's measured line ratios to estimate the increase in gas column density. However, the extra absorber might have a different, in particular a lower, line ratio. While we do not find any hint for such a change in the doublet line ratios, the data is insufficient to conclusively rule this possibility out. A ratio closer to unity would increase the column density corresponding to the EW increase. Based on the calculations by Strömgren (1948), we expect that this could increase the column density by about one order of magnitude. This would still be compatible with our upper limit from the low S/N Na UV absorption lines, which have oscillator strengths about a factor of 20 lower than the optical lines. The value of $EW \lesssim 0.7$ Å for the sum of both UV lines corresponds to an upper limit in the range of $\log N_{Na} \lesssim 15$ using the values by Strömgren (1948, the ratio between the optical and UV lines reduces to less than ten for strongly saturated optical lines). Higher S/N data with higher spectral resolution would allow one to confirm or rule out changes in the line ratio as well as to better constrain the gas column density using the UV lines.

Second, the elemental abundances (of the circumstellar material) might differ from the Sun's photospheric abundances. It is difficult to assess the error introduced by this effect as abundance patterns for circumstellar disks have not been measured. Studies of photospheric abundances in Herbig stars suggest a depletion in refractory elements, which has been related to dust filtering by planet formation within the protoplanetary disk (Kama et al. 2015). Extending this argument to volatile elements such as Na and K suggests that they could be overabundant so that a gas-to-dust ratio based on Na and K absorption would appear erro-

neously low. In principle, other species can be measured using, for example, UV transmission spectroscopy (in particular H), however, V 354 Mon is too dim to apply this method. Therefore, it is desirable to identify nearby systems with a stable AA Tau-like phenomenon and a (very) low accretion rate to avoid effects by accretion variability.

Third, our simple geometry used for calculating the photo-ionization might underestimate the ionization state of the plasma and a detailed model is needed to assess this possibility. We expect, however, that a more realistic structure rather reduces the ionization, because the high-energy photons would be efficiently absorbed in an outer, low density layer. Hence, fewer high-energy photons would reach the high density region in which the ionization conditions are closer to thermodynamic equilibrium. In total, we expect this to result in a lower average ionization.

Another possibility is that we overestimate the dust mass. However, our method is most prone to miss any large dust grains that do not cause reddening nor a significant dimming, and unlikely misses smaller dust that causes the optical reddening. Therefore, our dust estimate can be considered a lower limit so that our analysis strongly suggests a low gas-to-dust ratio in the disk warp, about 1:1. Factoring in the uncertainty in the gas column density, we still find strongly gas depleted material (perhaps up to roughly 10:1 gas-to-dust compared to 100:1 in the ISM). Such a gas depletion appears not unreasonable given the low accretion rate of V 354 Mon. Perhaps the disk is already evolving toward a debris disk and the lack of a sufficient reservoir of gas in the inner disk also causes the accretion rate to decrease.

6. Conclusions

Our analysis demonstrates that flux calibrated, broadband data such as X-Shooter spectra allow us to simultaneously determine the dust and gas properties. These properties, when combined with sufficient time sampling, provide access to the gas-to-dust ratio of disk warps that periodically partially occult the central star. We also describe how higher S/N data combined with better phase sampling can overcome limitations in the data analyzed here, which were obtained for a different purpose. Also, better phase sampling could reveal any phase differences between the dust and the gas as well as potentially allow a refined modeling of the height structure of the disk warp compared to our toy model with only three zones.

We find a gas-to-dust ratio for the inner disk regions around V 354 Mon that is a factor of ten or more lower than typical ISM values. One possibility is that V 354 Mon's disk is already evolving toward a debris disk, which could also be related to the low stellar accretion rate. Another mechanism possibly resulting in a low gas-to-dust ratio in the inner disk is the radial drift of large particles from the outer disk, which then fragment in the inner regions due to the high relative velocities (e.g., Birnstiel et al. 2010). Low gas-to-dust ratios in the inner disk might indicate that the streaming instability can be triggered in the proximity of the central star, leading to the formation of rocky cores at the $\lesssim$ au scale.

Better characterizing the properties of inner disk warps is also relevant in view of recent discoveries of shadows seen in very high spatial resolution scattered light images (e.g., Marino et al. 2015; Stolker et al. 2016; Juhász & Facchini 2017, for disks around HAeBe stars) or as rotating structures observed with HST, for example, for the nearby CTTSs TW Hya (Debes et al. 2017). An improved height model of the inner disk warp could address whether shadows seen in images of stellar light reflected at the disk surface might be related to the same disk warps that we studied in this paper. Combining complementary constraints for inner disk properties will eventually lead to a better understanding of the physical conditions in the terrestrial planet forming region.

Acknowledgements. PCS thanks Jerome Bouvier for interesting discussions and very valuable comments. Based on observations made with ESO Telescopes at the La Silla Paranal Observatory under programme ID 084.C-1095(A). PCS acknowledges support by DLR 50 OR 1307 and DFG SFB 676. PCS and CFM gratefully acknowledge ESA Research Fellowships, during which significant parts of the work were performed. DF acknowledges support from the Italian Ministry of Education, Universities and Research project SIR (RBSI14ZRHR). Support for HMG was provided by the National Aeronautics and Space Administration through Chandra Award Number GO6-17021X issued by the Chandra X-ray Observatory Center, which is operated by the Smithsonian Astrophysical Observatory for and on behalf of the National Aeronautics Space Administration under contract NAS8-03060.

References

Alcalá, J. M., Natta, A., Manara, C. F., et al. 2014, A&A, 561, A2
Alencar, S. H. P., Teixeira, P. S., Guimarães, M. M., et al. 2010, A&A, 519, A88
Ansdell, M., Gaidos, E., Williams, J. P., et al. 2016, MNRAS, 462, L101
Birnstiel, T., Dullemond, C. P., & Brauer, F. 2010, A&A, 513, A79
Bouvier, J., Alencar, S. H. P., Harries, T. J., Johns-Krull, C. M., & Romanova, M. M. 2007, Protostars and Planets V, 479
Bouvier, J., Chelli, A., Allain, S., et al. 1999, A&A, 349, 619
Bouvier, J., Grankin, K., Ellerbroek, L. E., Bouy, H., & Barrado, D. 2013, A&A, 557, A77
Bouvier, J., Grankin, K. N., Alencar, S. H. P., et al. 2003, A&A, 409, 169
Bozhinova, I., Scholz, A., Costigan, G., et al. 2016, MNRAS, 463, 4459
Cardelli, J. A., Clayton, G. C., & Mathis, J. S. 1989, ApJ, 345, 245
Cox, E. G., Harris, R. J., Looney, L. W., et al. 2017, ApJ, 851, 83
Dahm, S. E. 2008, The Young Cluster and Star Forming Region NGC 2264, ed. B. Reipurth, 966
Dahm, S. E., Simon, T., Proszkow, E. M., & Patten, B. M. 2007, AJ, 134, 999
Debes, J. H., Poteet, C. A., Jang-Condell, H., et al. 2017, ApJ, 835, 205
Facchini, S., Manara, C. F., Schneider, P. C., et al. 2016, A&A, 596, A38
Ferland, G. J., Porter, R. L., van Hoof, P. A. M., et al. 2013, Rev. Mexicana Astron. Astrofis., 49, 137
Fűrész, G., Hartmann, L. W., Szentgyorgyi, A. H., et al. 2006, ApJ, 648, 1090
Fischer, W., Kwan, J., Edwards, S., & Hillenbrand, L. 2008, ApJ, 687, 1117
Flaccomio, E., Micela, G., & Sciortino, S. 2006, A&A, 455, 903
Fonseca, N. N. J., Alencar, S. H. P., Bouvier, J., Favata, F., & Flaccomio, E. 2014, A&A, 567, A39
Foucart, F. & Lai, D. 2011, MNRAS, 412, 2799
France, K., Schindhelm, E., Bergin, E. A., Roueff, E., & Abgrall, H. 2014, ApJ, 784, 127
Hamilton, C. M., Herbst, W., Shih, C., & Ferro, A. J. 2001, ApJ, 554, L201
Husser, T.-O., Wende-von Berg, S., Dreizler, S., et al. 2013, A&A, 553, A6
Juhász, A. & Facchini, S. 2017, MNRAS, 466, 4053
Kama, M., Folsom, C. P., & Pinilla, P. 2015, A&A, 582, L10
Lamm, M. H., Bailer-Jones, C. A. L., Mundt, R., Herbst, W., & Scholz, A. 2004, A&A, 417, 557
Long, F., Herczeg, G. J., Pascucci, I., et al. 2017, ApJ, 844, 99
Loomis, R. A., Öberg, K. I., Andrews, S. M., & MacGregor, M. A. 2017, ApJ, 840, 23
Manara, C. F., Beccari, G., Da Rio, N., et al. 2013, A&A, 558, A114
Manara, C. F., Fedele, D., Herczeg, G. J., & Teixeira, P. S. 2016, A&A, 585, A136
Marino, S., Perez, S., & Casassus, S. 2015, ApJ, 798, L44
Matt, S. P., Pinzón, G., de la Reza, R., & Greene, T. P. 2010, ApJ, 714, 989
McGinnis, P. T., Alencar, S. H. P., Guimarães, M. M., et al. 2015, A&A, 577, A11
Modigliani, A., Goldoni, P., Royer, F., et al. 2010, in Proc. SPIE, Vol. 7737, Observatory Operations: Strategies, Processes, and Systems III, 773728
Nomura, H., Tsukagoshi, T., Kawabe, R., et al. 2016, ApJ, 819, L7
Pascucci, I., Edwards, S., Heyer, M., et al. 2015, ApJ, 814, 14
Petrov, P. P., Gahm, G. F., Djupvik, A. A., et al. 2015, A&A, 577, A73
Rodriguez, J. E., Pepper, J., Stassun, K. G., et al. 2015, AJ, 150, 32
Rodriguez, J. E., Zhou, G., Cargile, P. A., et al. 2017, ApJ, 836, 209
Rugel, M., Fedele, D., & Herczeg, G. 2018, A&A, 609, A70
Scaringi, S., Manara, C. F., Barenfeld, S. A., et al. 2016, MNRAS, 463, 2265
Schneider, P. C., France, K., Günther, H. M., et al. 2015a, A&A, 584, A51
Schneider, P. C., Günther, H. M., Robrade, J., et al. 2015b, A&A, 584, L9
Siess, L., Dufour, E., & Forestini, M. 2000, A&A, 358, 593
Stauffer, J., Cody, A. M., McGinnis, P., et al. 2015, AJ, 149, 130
Stolker, T., Dominik, C., Avenhaus, H., et al. 2016, A&A, 595, A113
Strömgren, B. 1948, ApJ, 108, 242
Venuti, L., Prisinzano, L., Sacco, G. G., et al. 2018, A&A, 609, A10
Welty, D. E. & Hobbs, L. M. 2001, ApJS, 133, 345

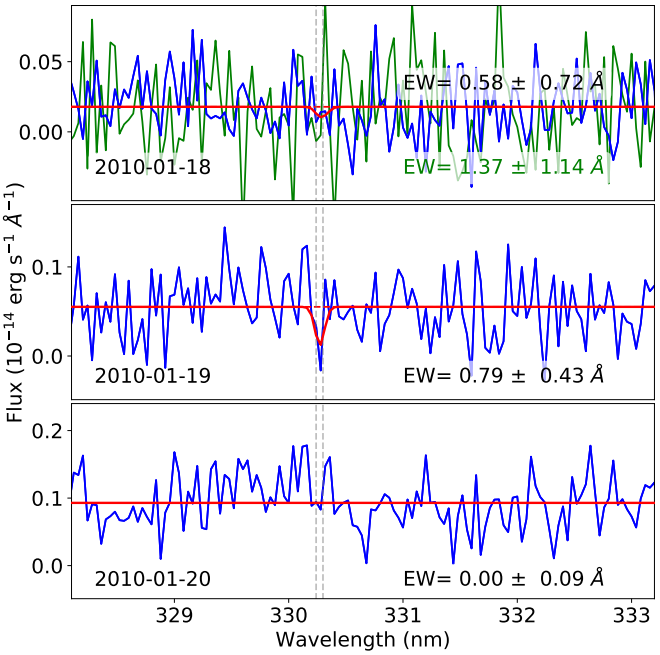


Fig. A.1. Na UV absorption lines with the locations of the lines plotted. The red line indicates the best fit model (to the longer spectrum for 2010-01-18).

Appendix A: Veiling

We inspected the line depth in several wavelength regions accros the optical spectrum. We then calculated a pseudo equivalent width as

$$\int_{\lambda_0}^{\lambda_1} 1 - F_{norm}(\lambda) d\lambda \,. \tag{A.1}$$

These pseudo equivalents are provided in Fig. B.1.

Appendix B: Input spectrum for `cloudy` simulations

The cloudy simulations need a reasonable input spectrum that includes the high-energy portion of the stellar spectrum. We constructed such a spectrum based on, first, the flux calibrated X-Shooter spectrum for the optical part, second, the RECX 11 FUV spectrum from France et al. (2014, RECX 11 is a weakly accreting K4 similar to V 354 Mon), and third, X-ray data published by Dahm et al. (2007, $\log L_X = 30.61$). We then interpolated a solar spectrum to fill the EUV part of the spectrum using a first order polynomial fixed at the two connecting points (X-ray/FUV). The long wavelength part ($\lambda \gg 1\,\mu$m) of the spectrum was approximated by a blackbody. We experimented with several normalizations but found the effects to be on the same order as mild changes in the (unknown) gas-to-dust ratio of the inner disk rim. We therefore used $L = 4 \times 10^{33}$ erg s^{-1}, which matches the flux calibrated X-Shooter spectrum.

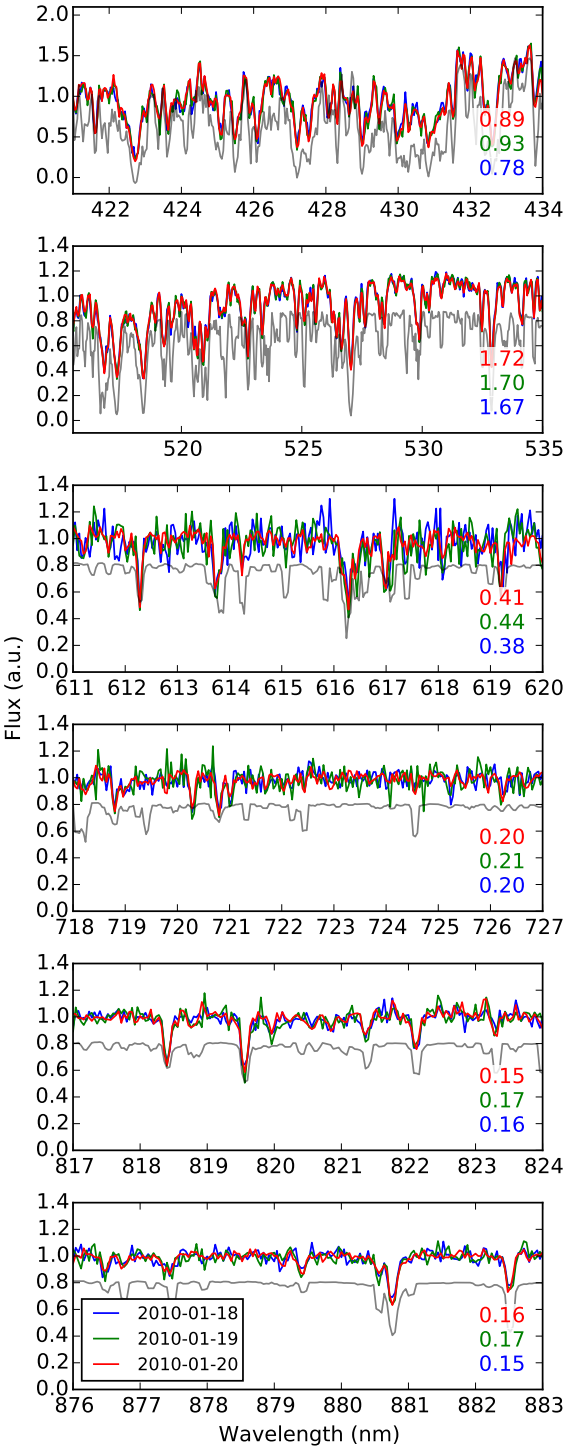


Fig. B.1. Stellar features at different wavelengths accross the spectral range of X-Shooter. A synthetic spectrum is overlayed in gray but offset by 0.2 for clarity. Numbers indicate the pseudo equivalent width calculated over the displayed wavelength region.